

Kinetic energy and spin-orbit splitting in nuclei near neutron drip line

I.Hamamoto^a, S.V.Lukyanov^{a,b} and X.Z.Zhang^{a,c}

^a Department of Mathematical Physics

Lund Institute of Technology at University of Lund
Lund, Sweden.

^b Institute for Nuclear Research of the National Academy of Sciences
Kiev, Ukraine

^c Institute of Atomic Energy, Beijing
The People's Republic of China.

ABSTRACT : Two important ingredients of nuclear shell-structure, kinetic energy and spin-orbit splitting, are studied as a function of orbital angular momenta ℓ and binding energies, when binding energies of neutrons decrease towards zero. If we use the standard parameters of the Woods-Saxon potential in β stable nuclei and approach the limit of zero binding energy from 10 MeV, the spin-orbit splitting for $n=1$ orbitals decreases considerably for $\ell=1$, while for $\ell>2$ little decreasing is observed in the limit. In contrast, the kinetic energy decreases considerably for $\ell \lesssim 3$. The smaller the ℓ values of orbitals, the larger the decreasing rate of both kinetic energy and spin-orbit splitting. The dependence of the above observation on the diffuseness of potentials is studied.

PACS numbers : 21.10.Pc

1 Introduction

One-particle shell structure is well studied for nuclei along the β stability line. Using recent radioactive nuclear ion beam facilities it has become possible to study the structure of exotic nuclei away from the β stability line, in which least-bound nucleons have much smaller separation energies compared with those in β stable nuclei. Some interesting change of shell structure is expected and/or observed, when we move away from β stable nuclei to drip line nuclei. This change is made due to the presence of loosely-bound nucleons as well as exotic values of isospin for a given mass number. For example, available experimental information on the nucleus $^{32}_{12}\text{Mg}_{20}$, which is a singly-closed-shell nucleus in the traditional terminology, seems to indicate that the nucleus is deformed [1, 2]. Furthermore, the creation of a new magic number $N=16$ near the neutron drip line ($T_z \geq 3$) is recently suggested [3]. In the present work we study the two basic ingredients of nuclear shell-structure, kinetic energy and spin-orbit splitting, for relatively simple potentials, having the spirit similar to that of ref. [4]. In available publications certain aspects of shell structure unique in drip line nuclei have been studied using self-consistent Hartree-Fock (HF) calculations of various types.

Using Skyrme-type HF calculations, in ref. [5] we have studied neutron one-particle level scheme with a fixed mass number as a function of neutron number, including one-particle resonant levels. It is seen that calculated one-particle levels with lower ℓ are systematically pushed down relative to those with higher ℓ , as we approach the neutron drip line. On the other hand, in ref. [6] the reduction of the spin-orbit potential in light neutron rich nuclei, especially the isospin-dependence of the spin-orbit term is discussed, using the relativistic mean field theory. In the Skyrme-type HF calculations of ref. [7] it is found that the estimated $1\text{p}_{1/2}-1\text{p}_{3/2}$ spin-orbit splitting of the light mirror nuclei, $^8_6\text{C}_2$ and $^8_2\text{He}_6$, is about 30 percent smaller than the one in the β stable nucleus $^{12}_6\text{C}_6$. The difference of the isospin-dependence of spin-orbit term in the relativistic and traditional Skyrme-type HF calculations is certainly important [8] to be examined.

A systematic study of both kinetic energy and spin-orbit splitting as a function of one-particle binding energy, orbital angular momentum and the shape of the potential is essential in understanding the variation of the shell structure as we approach the drip lines. In self-consistent HF calculations not only the orbitals with less binding energies are occupied but also the effective diffuseness of one-body potentials is changed due to the occupation, as we approach the drip lines. In the following the variation of shell structure is studied for potentials with a given diffuseness. We note that in usual shell model calculations harmonic oscillator wave functions are used and single-particle energies are input parameters. In order to give appropriate input parameters for nuclei away from the β stability line, it is important to know characteristic features of both the variation of kinetic energy and that of the strength of spin-orbit potential when approaching the drip lines. In ref. [9] the isospin-dependence of kinetic energies in light neutron-rich nuclei is suggested to be used in shell-model calculations. We will later comment on this suggestion. In the present work we limit ourselves to the study of lighter nuclei, since at the moment experimental data on nuclei close to the neutron drip line may be obtained only for lighter nuclei.

In Fig. 1a we plot one-particle energy eigenvalues for neutrons in the Woods-Saxon potential

$$U_{ws}(r) = -\frac{U_0}{1 + \exp(\frac{r-R}{a})} \quad (1)$$

together with the spin-orbit potential

$$U_{so} = -v \left(\frac{\lambda_c}{2}\right)^2 \frac{1}{r} \frac{dU_{ws}(r)}{dr} (\vec{\ell} \cdot \vec{s}) \quad (2)$$

choosing the 1p, 2s, 1d, 2p and 1f orbitals. In the expression (2) λ_c expresses the nucleon Compton wave-length. Used parameters are

$$\begin{aligned} R &= r_0 A^{1/3} & \text{with} & \quad r_0 = 1.27 \text{ fm} \\ a &= 0.67 \text{ fm} & & \quad (3) \end{aligned}$$

and $N=Z$ in the depth of the Woods-Saxon potential

$$U_0 = \left(50 - 32 \frac{N - Z}{A} \right) \text{ MeV} \quad (4)$$

and in the strength of the spin-orbit potential [10],

$$v = \left(32 - 20 \frac{N - Z}{A} \right) \quad (5)$$

The energies of neutron orbitals calculated using almost the same parameters as in Fig. 1a are found for $A>20$ in p.239 of ref. [10]. Due to the presence of less-bound neutrons the diffuseness of the potential may become larger as we approach neutron drip lines. However, just using a larger diffuseness may not always correspond to the realistic situation. This is partly because the major part of the total potential comes from the core particles, which are well bound and are the majority. Furthermore, it is partly because the proton core, which makes a more important contribution to the neutron potential than the neutron core, is more deeply bound in nuclei closer to neutron drip lines. As a numerical example with a larger diffuseness, in Fig. 1b we show the one-particle energy eigenvalues for the Woods-Saxon potential with the same parameters as those used in Fig. 1a except for doubling the diffuseness, $a=1.34$ fm.

In Figs. 1a and 1b we observe : (a) the A -dependence of the eigenvalues $E_{n\ell}$ in the energy region of $E_{n\ell} \gtrsim -15$ MeV depends very much on the orbital angular momentum ; (b) as is seen, for example, from the crossing of the eigenvalues of $1d_{5/2}$ and $2s_{1/2}$ orbitals at $E_{n\ell}=-0.71$ MeV in Fig. 1a and $E_{n\ell}=-7.21$ MeV in Fig. 1b, it is known that the slope of eigenvalues for lower ℓ orbitals becomes relatively much less, as the eigenvalues approach zero ; (c) The spin-orbit splitting with a given (n, ℓ) may generally be expected to become larger ($\sim A^{-1/3}$) as the mass number decreases. In contrast, the spin-orbit splitting between $1p_{1/2}$ and $1p_{3/2}$ (or $2p_{1/2}$ and $2p_{3/2}$) does not increase but it rather decreases when $E_{n\ell}$ goes up from -5 to 0 MeV. In Fig. 1b the decrease is observed also for the spin-orbit splitting of $1d$ orbitals; (d) For the potential with a larger diffuseness the features mentioned above, (a)-(c), are more pronounced. We note that the prominent

difference of one-particle shell structure, such as the level order and the energy gap, between Figs. 1a and 1b is observed especially for $E_{n\ell} \gtrsim -10$ MeV.

In ref. [11] we studied the coupling of particles near threshold to shape oscillations and showed the evaluated matrix elements of

$$V_{pv}(r) = R \frac{dU(r)}{dr} \quad (6)$$

where $U(r)$ expresses the one-particle potential while R represents the nuclear radius. Noting that the kinetic energy of the spherical system in the absence of spin-orbit potential is equal to the expectation value of

$$\frac{r}{2} \frac{dU(r)}{dr} \quad (7)$$

due to the virial theorem, for the square-well potential the expectation value of (6) is equal to twice the kinetic energy. Furthermore, the expectation value of

$$\frac{1}{r} \frac{dU(r)}{dr} \quad (8)$$

which is the radial dependence of the spin-orbit potential, is equal to $1/R^2$ times that of (6) in the case of the square-well potential. Thus, for the square-well potential Fig. 3a of ref. [11] already contains all information on both the kinetic energy and the spin-orbit splitting. In the present work we investigate those two quantities for Woods-Saxon potentials compared with the square-well potential, studying the dependence on energy especially for $E_{n\ell} = -10 \rightarrow 0$ MeV and on angular momenta. Though it can be disputed whether the radial derivative of the density or that of the potential should be used for the radial dependence of the spin-orbit potential, for simplicity we use the form in (8).

In sect.2 we present numerical results and discussions, while conclusions are given in sect.3.

2 Numerical results and discussions

In the present section we do not include the spin-orbit potential in the one-body potential, for simplicity. We evaluate the expectation value of the operators,

$$\frac{r}{U_0} \frac{dU(r)}{dr} \quad (9)$$

and

$$\frac{1}{r U_0} \frac{dU(r)}{dr} \quad (10)$$

for neutron orbitals in Woods-Saxon potentials. The expectation values of (9) is equal to those plotted in Fig. 3a of [11] in the case of the square-well potential. Note that the quantity on the x-axis in Fig. 3a of ref. [11] for the square-well potential has the same meaning as that on the x-axis in Fig. 2 and 3 of the present paper, though the notation used for the square-well potential in ref. [11] was different. The expectation value of (9) is proportional to the kinetic energy, while that of (10) to the spin-orbit splitting for a given orbital angular momentum ℓ treating the spin-orbit potential by perturbation. We examine those expectation values for a given (n, ℓ) value as a function of $E_{n\ell}/U_0$ where $E_{n\ell}$ expresses one-particle energy eigenvalues.

In Figs. 2a and 2b the expectation value of the operator (9) is plotted for the Woods-Saxon potential with the diffuseness $a=0.67$ and 1.34 fm, respectively, while in Fig. 2c we show the same quantity for the square-well potential,

$$U(r) = \begin{cases} -U_0 & \text{for } r < R \\ 0 & \text{for } r \geq R \end{cases} \quad (11)$$

a part of which was taken from Fig. 3a of ref. [11]. In the limit of infinite square-well potential ($U_0 \rightarrow \infty$), the kinetic energy is equal to $U_0 + E_{n\ell}$ and, thus, the expectation value of (9) multiplied by U_0 is given by $2(U_0 + E_{n\ell})$ for all orbitals with various (n, ℓ) values. The expectation value for the infinite square-well potential is shown in Fig. 2c by the thin straight line. Since the relation between the quantities in the x- and y-axis multiplied by U_0 is expressed by a straight line, dividing both quantities by any given “ U_0 ” does

not change the straight line. Thus, we plot the line for the infinite square-well potential also in Fig. 2c. Note that one-particle wave-functions cannot extend to outside of the potential with $U_0 \rightarrow \infty$ and, thus, the reduction in the increasing rate of kinetic energy does not occur as $(1+(E_{n\ell}/U_0))$ increases.

It should be noted that along the curve with a given (n,ℓ) the mass number monotonically decreases as $(1+(E_{n\ell}/U_0))$ increases. For a very large value of U_0 , one may approximately write (see eq. (13))

$$U_0 + E_{n\ell} = \frac{c_{n\ell}}{R^2} \quad (12)$$

where $c_{n\ell} > 0$, $U_0 > 0$ and $E_{n\ell} < 0$, while R expresses the radius of the system. Thus, in order to obtain larger eigenvalues $E_{n\ell}$, namely larger values of $(1+(E_{n\ell}/U_0))$, keeping a fixed value of U_0 , one must decrease values of R (or the mass number A).

The vertical dotted line of Fig. 2 at $1+(E_{n\ell}/U_0)=0.8$, namely $E_{n\ell}=-10$ MeV for $U_0=50$ MeV, indicates the approximate Fermi level in β stable nuclei. When the eigenvalue $E_{n\ell} \rightarrow 0$ exists for the potential with a finite range, the expectation value of (9) for $(n, \ell=0)$ orbitals in the finite-well potential approaches zero, since due to the absence of centrifugal barrier the $\ell=0$ neutron wave functions can extend up to infinity. For the square-well potential the expectation value of (9) at $E_{n\ell}=0$ is independent of n and is equal to $2/3$, $6/5$ and $10/7$, for the $\ell=1$, 2 and 3 orbitals, respectively [11]. In contrast, the expectation value for Woods-Saxon potentials depends on radial node n and is almost a factor two (four) smaller for the potential in Fig. 2a (2b). It is also noted that for more diffuse potentials the absolute magnitude of kinetic energy of a given (n, ℓ) orbital is considerably smaller for almost all values of $E_{n\ell}$.

The effect of the diffuse surface of the potential on kinetic energy is seen from the comparison of the curves in Figs. 2a and 2b with those in Fig. 2c for the finite and infinite square-well potential. The considerable deviation from the straight line occurs first at smaller values of $|E_{n\ell}|$ for less diffuse potential and for larger ℓ orbitals. In other words, the kinetic energy starts to decrease already at relatively larger binding energy

for more diffuse potentials. This is because for more diffuse potentials the wave functions can more easily extend to the outside of the potentials. The extension is easier for the orbitals with smaller orbital angular momenta because of the lower centrifugal barriers. As seen in Fig. 2c, for the square-well potential the kinetic energy starts to decrease first at very small binding energies, even for $\ell=0$ orbitals.

The deviation of kinetic energy of (n, ℓ) orbitals from the monotonic increase as $E_{n\ell}$ increases from -10 to 0 MeV depends somewhat on the radial node n . The larger the quantum number n , the larger the variation of the kinetic energy for $E_{n\ell} = -10 \rightarrow 0$ MeV. This is understood because at $(1+E_{n\ell}/U_0)=0.8$, namely $E_{n\ell}=-10$ MeV, the kinetic energy of orbitals with larger n is larger than that with smaller n , while at $E_{n\ell}=0$ the kinetic energy of orbitals with a given ℓ is almost independent of n . The latter is independent of n for the square-well potential.

In ref. [9] the isospin dependence of kinetic energies in very light neutron-rich nuclei is suggested, in which the isospin dependence for the $2s_{1/2}$ and $1d_{3/2}$ state is taken to be the same as that for the $1d_{5/2}$ state. The origin of the isospin-dependence is certainly traced back to the decreasing binding energy of least bound neutrons as well as the possible larger surface diffuseness of the potential, when the isospin increases in those light neutron-rich nuclei. However, from our study shown in Fig. 2 we note that the binding-energy dependence of kinetic energy for the $2s$ and $1d$ states are very different for a given potential, especially for $E_{n\ell} = -10 \rightarrow 0$ MeV. Observe the difference of the behaviour between the solid and dashed curve in Fig. 2 for $(1+E_{n\ell}/U_0)=0.8 \rightarrow 1.0$.

In Figs. 3a and 3b the expectation value of the operator (10) is plotted for the Woods-Saxon potential with the diffuseness $a=0.67$ and 1.34 fm, respectively, while in Fig. 3c we show the same quantity for the square-well potential. For the square-well potential the expectation value of (10) depends on some extra parameter to specify, either U_0 or R , other than the only parameters unique in the model, U_0R^2 and $E_{n\ell}R^2$ [12]. We have used $U_0=50$ MeV.

The thin curves in Fig. 3c are estimated for the infinite square-well potential. For the ($U_0 \rightarrow \infty$) square-well potential the kinetic energy is equal to

$$U_0 + E_{n\ell} = \frac{\hbar^2 x_{n\ell}^2}{2 M R^2} \quad (13)$$

where $x_{n\ell}$ expresses the n -th zero point of the spherical Bessel function $j_\ell(z)$. Thus, the expectation value of the operator in (10) multiplied by U_0 is written as

$$\frac{2(U_0 + E_{n\ell})}{R^2} = \frac{4 M (U_0 + E_{n\ell})^2}{\hbar^2 x_{n\ell}^2}. \quad (14)$$

Variables in the x- and y-axis in Fig. 3c are those in (13) and (14) divided by “ U_0 ”, however, the division by “ U_0 ” = ∞ does not make sense. Since the relation between the quantities in (13) and (14) is not linear, the shape of the curve depends on the “ U_0 ” value used for evaluating variables in the x- and y-axis. Since our purpose is to compare the result of finite potentials with that of the infinite potential, we choose this “ U_0 ” value so that at $(1+(E_{n\ell}/U_0))=0.8$ the thin curve coincides with the corresponding curve for the finite square-well potential. It is seen that only in the region $(1+(E_{n\ell}/U_0)) \gtrsim 0.8$ the curve for the finite square-well potential differs appreciably from that for the infinite square-well potential.

The plotted quantity in Fig. 3 times $(2\ell+1)$ is proportional to the spin-orbit splitting. For a given $E_{n\ell}$ value the spin-orbit splitting for the 1p orbital is much larger than that for the 2p orbital, since the former belongs to lighter nuclei. For the purpose of comparison of expectation values of (10), we plotted calculated values also for 2s orbitals, though no spin-orbit potential acts on s-orbitals.

The diffuse surface effect of potentials on spin-orbit splitting is seen from the comparison of curves in Figs. 3a and 3b with those in Fig. 3c for the finite and infinite square-well potential. Due to the different r-dependence, the effect of the diffuse surface on kinetic energy starts to appear already at deeper bound orbitals compared with spin-orbit splitting. As already exhibited in Fig. 1b, for the Woods-Saxon potential with $a=1.34$ fm the spin-orbit splitting of 1d orbitals decreases also appreciably as $E_{n\ell}$ changes from -10

to 0 MeV. The decrease corresponds to the variation of the dashed curve in Fig. 3b for $(1+E_{n\ell}U_0)=0.8\rightarrow1.0$.

The variation of spin-orbit splitting of orbitals with a given ℓ for $E_{n\ell}=-10\rightarrow0$ MeV depends moderately on the radial node n . We also note that the comparison of spin-orbit splittings of the orbitals with a given ℓ but with different n means the comparison made for nuclei with different mass number.

In order to simulate the spin-orbit potential in which the radial derivative of the density is used instead of that of the potential, we have also made the numerical calculation using $r_0=(0.9)(1.27)=1.14$ fm in $U(r)$ of (10) while keeping one-particle wave-functions unchanged. The dependence of the expectation value of (10) on either ℓ or n for $E_{n\ell}=-10\rightarrow0$ MeV is found to be almost the same as what is described above.

3 Conclusions

In order to study the variation of one-particle shell-structure due to the surface diffuseness of nuclear potential, the radial matrix-elements of both kinetic energy and spin-orbit potential of Woods-Saxon potentials are estimated and compared with those of the infinite and finite square-well potential. We are especially interested in the energy region where binding energies of neutrons decrease from 10 to 0 MeV, having nuclei close to neutron drip lines in mind. In the infinite square-well potential neither kinetic energy nor spin-orbit splitting ever decreases as a function of $E_{n\ell}$. For the finite square-well potential with $U_0=50$ MeV a decrease is observed for $E_{n\ell}=-10\rightarrow0$ MeV, depending on orbitals. For orbitals with smaller ℓ values both quantities decrease more strongly as binding energies approach zero. The decrease is stronger for more diffuse potentials. Due to the different r -dependence, the effect of the diffuse surface on kinetic energy starts to appear already at deeper bound orbitals compared with spin-orbit splitting.

In traditional shell model calculations carried out for neutron drip line nuclei, it is important to take into account the variation of both kinetic energy and spin-orbit split-

ting in the input one-particle energies, which is studied in the present work. Not only the binding energy dependence of those quantities but also the ℓ dependence is very important.

Acknowledgements

X.Z.Z. acknowledges the financial support provided by Crafoordska Stiftelsen, while S.V.L. is grateful to The Royal Swedish Academy of Sciences for the financial support under the contract for cooperation between Sweden and the former Soviet Union.

References

- [1] D.Guillemaud-Mueller et al., Nucl. Phys. **A426** (1984) 37.
- [2] T.Motobayashi et al., Phys. Lett. **B346** (1995) 9.
- [3] A. Ozawa, T. Kobayashi, T. Suzuki, K. Yoshida and I. Tanihata, Phys. Rev. Lett., in print.
- [4] F. Catara, C. H. Dasso and A. Vitturi, Nucl. Phys. **A602** (1996) 181.
- [5] I. Hamamoto, H. Sagawa and X. Z. Zhang, Phys. Rev. **C53** (1996) 765.
- [6] G. A. Lalazissis, D. Vretenar, W. Poschl and P. Ring, Phys. Lett. **B418** (1998) 7.
- [7] I. Hamamoto and H. Sagawa, Phys. Rev. **C60** (1999) 064314.
- [8] P. -G. Reinhard and H. Flocard, Nucl. Phys. **A584** (1995) 467.
- [9] H. Kitagawa and H. Sagawa, Nucl. Phys. **A551** (1993) 16.
- [10] A. Bohr and B. R. Mottelson, Nuclear Structure, Vol.I (Benjamin, Reading. MA, 1969).

- [11] I. Hamamoto and X. Z. Zhang, Phys. Rev. **C58** (1998) 3388.
- [12] K. Riisager, A. S. Jensen and P. Moller, Nucl. Phys. **A548** (1992) 393.

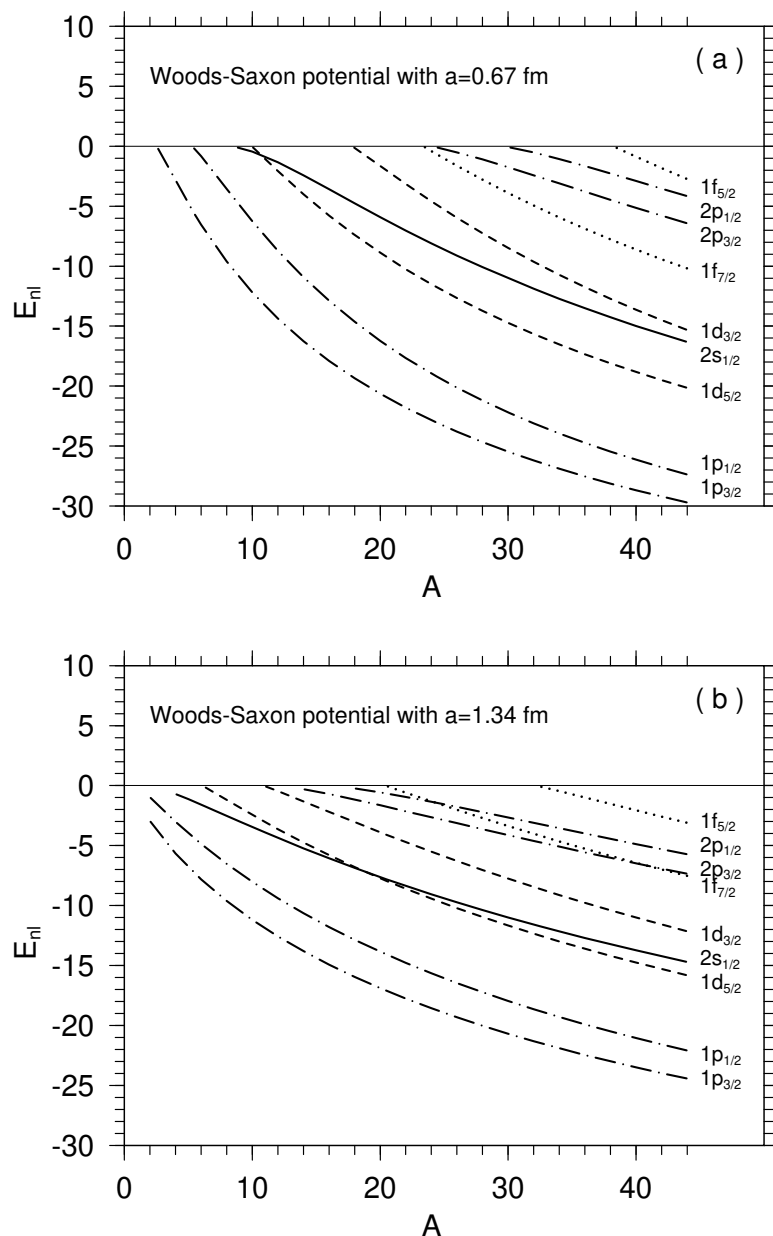


Figure 1: Energies of neutron orbits : (a) for the Woods-Saxon potential with parameters, (3), (4), (5) and $N=Z$; (b) the same as (a) except for $a=1.34$ fm.

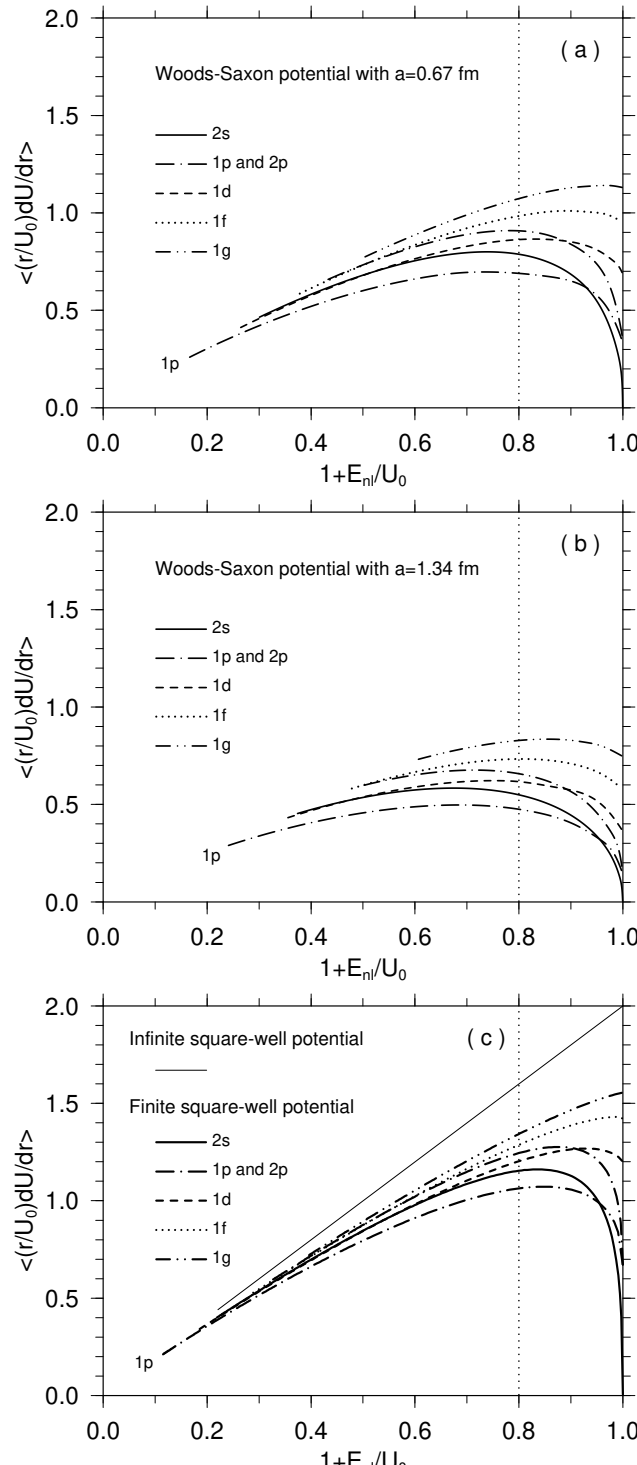


Figure 2: The expectation values of the operator (9), which is proportional to kinetic energy of respective one-particle orbitals, as a function of $(1+(E_{nl}/U_0))$ where E_{nl} expresses the one-particle energy eigenvalue of the orbital (n, ℓ) . For $U_0=50$ MeV $(1+(E_{nl}/U_0))=0.8$ and 1.0 mean $E_{nl}=-10$ and 0 MeV, respectively. (a) for the Woods-Saxon potential with parameters, (3), (4), $v=0$ and $N=Z$; (b) the same as (a) except for $a=1.34$ fm ; (c) for the square-well potential (11). By the thin straight line in Fig. 2c the expectation value of the operator (9) is exhibited for the infinite square-well potential. The thin line is the same for all orbitals with various (n, ℓ) values. See the text for details.

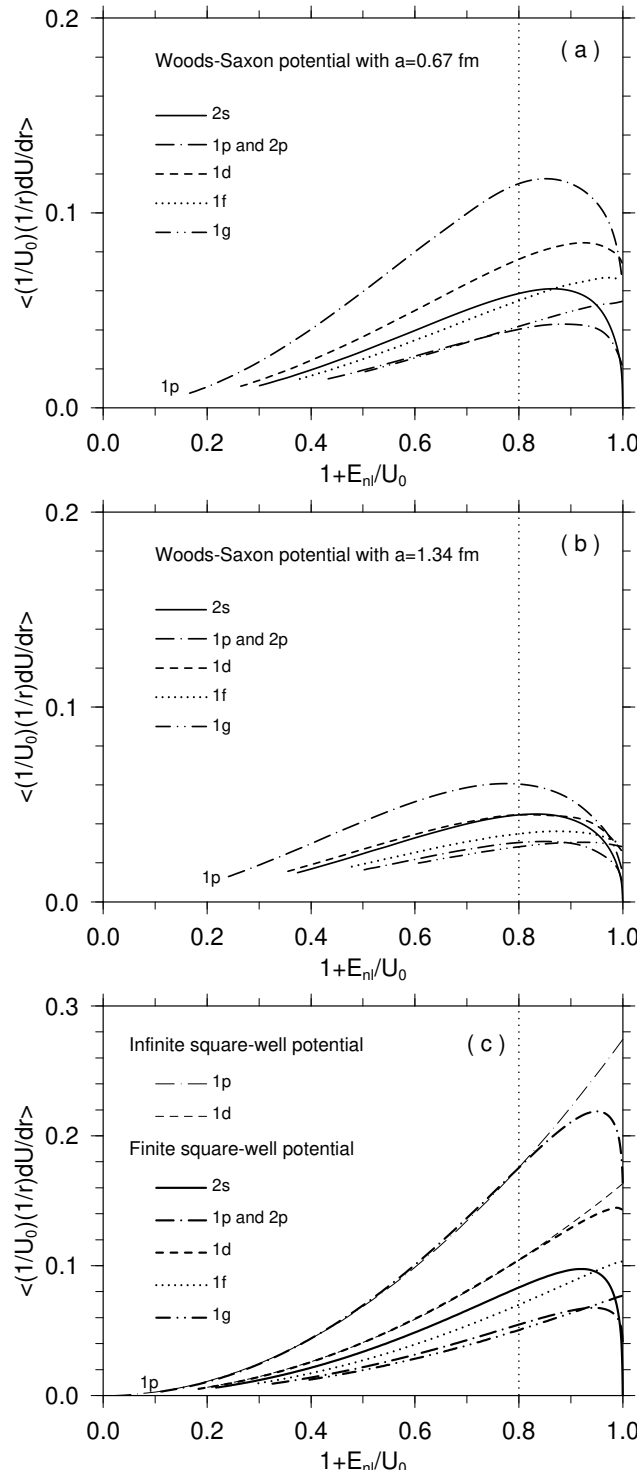


Figure 3: The expectation values of the operator (10), which in the perturbation treatment of spin-orbit potential is proportional to the spin-orbit splitting of the ℓ orbital when multiplied by $(2\ell+1)$, as a function of $(1+(E_{nl}/U_0))$. For $U_0=50$ MeV $(1+(E_{nl}/U_0))=0.8$ and 1.0 mean $E_{nl}=-10$ and 0 MeV, respectively. (a) for the Woods-Saxon potential with parameters, (3), (4), $v=0$ and $N=Z$; (b) the same as (a) except for $a=1.34$ fm ; (c) for the square-well potential (11) with $U_0=50$ MeV. By the thin curves in Fig. 3c the expectation value in the infinite square-well potential is shown for the 1p and 1d orbitals. See the text for details.